Available online at www.sciencedirect.com
ScienceDirect
International Journal of Heat and Mass Transfer 50 (2007) 1790–1804
International Journal of HEAT and MASS TRANSFER
www.elsevier.com/locate/ijhmt

# Numerical and experimental study of melting in a spherical shell

E. Assis, L. Katsman, G. Ziskind *, R. Letan

*Heat Transfer Laboratory, Department of Mechanical Engineering, Pearlstone Center for Aeronautical Studies, Ben-Gurion University of the Negev, P.O.Box 653, Beer-Sheva 84105, Israel*

Received 8 January 2006; received in revised form 24 August 2006
Available online 28 November 2006

**Abstract**

The present study explores numerically and experimentally the process of melting of a phase-change material (PCM) in spherical geometry. Its properties used in the simulations, including the melting temperature, latent and sensible specific heat, thermal conductivity and density in solid and liquid states, are based on a commercially available paraffin wax, which is manufactured to be used mainly in latent-heat-based heat storage systems. A detailed parametric investigation is performed for melting in spherical shells of 40, 60, and 80 mm in diameter, when the wall-temperature is uniform and varies from 2 °C to 20 °C above the mean melting temperature of the PCM. Transient numerical simulations are performed using the Fluent 6.0 software. These simulations show the melting process from the beginning to the end, and incorporate such phenomena as convection in the liquid phase, volumetric expansion due to melting, sinking of the solid in the liquid, and close contact melting. The results of the experimental investigation, which included visualization, compare favorably with the numerical results and thus serve to validate the numerical approach. The computational results show how the transient phase-change process depends on the thermal and geometrical parameters of the system, including the temperature difference between the wall and the mean melting temperature, and the diameter of the shell. Dimensional analysis of the results is performed and presented as the mean Nusselt numbers and PCM melt fractions vs. an appropriate combination of the Fourier, Stefan, and Grashof numbers. This analysis leads to generalization which encompasses the cases considered herein.


*Keywords:* Melting; PCM; Simulation; Dimensional analysis; Correlation

## 1. Introduction

Phase-change in spherical geometry is of great interest both from the theoretical point of view and for the development of heat storage systems based on the use of latent-heat. A considerable amount of literature on this subject reflects experimental, theoretical, and numerical investigations undertaken in the past [1], while active work in the field continues, e.g. [2,3].

The processes of phase-change are not the same for different materials. For example, melting of ice is determined by the fact that it is lighter than water [4,5]. When an enclosed ice sphere melts, the total volume decreases. The solid fraction floats at the surface of the melt water and touches the inside surface of the sphere. A spherical shape of the solid fraction is retained for most of the melting process except towards the end when it loses its spherical shape and becomes flattened or elongated until melting is completed. On the other hand, when the solid is denser than the liquid, it is expected that the solid bulk, if it is not fixed, will move vertically downward. The motion of the solid bulk is accompanied by generation of liquid at the melting interface. This liquid is squeezed up through a narrow gap between the melting surface and the wall of the shell, to the space above the solid. The effect of solid phase sinking and appearance of "close contact melting" [6] is very significant. The literature shows that when the solid is fixed by some mechanical obstacle, both melting patterns and qualitative characteristics of the process become entirely different, as shown by Rieger et al. [7], Khodadadi and Zhang [8], Katayama et al. [9]. It is worth to note that such result

* Corresponding author. Tel.: +972 8 647 7089; fax: +972 8 647 2813.
*E-mail address:* gziskind@bgumail.bgu.ac.il (G. Ziskind).

0017-9310/$ - see front matter © 2006 Elsevier Ltd. All rights reserved.
doi:10.1016/j.ijheatmasstransfer.2006.10.007

**Nomenclature**

| | |
|---|---|
| $c_p$ | specific heat at constant pressure (J/kg °C) |
| $D$ | diameter (m) |
| $Fo$ | Fourier number $(k/\rho c_p)(t/R^2)$ |
| $Gr$ | Grashof number $(g\rho^2\beta\Delta T R^3/\mu^2)$ |
| $\hbar$ | enthalpy (J/kg) |
| $h$ | heat transfer coefficient (W/m$^2$ °C) |
| $k$ | thermal conductivity (W/m °C) |
| $L$ | latent heat (J/kg) |
| $Nu$ | Nusselt number $(q''/\Delta T)(R/k)$ |
| $Pr$ | Prandtl number $(c_p\mu/k)$ |
| $q''$ | heat flux (W/m$^2$) |
| $R$ | radius (m) |
| $Ste$ | Stefan number $(c_p\Delta T/L)$ |
| $t$ | time (s) |
| $T$ | temperature (°C or K) |
| $u$ | velocity component (m/s) |
| $x$ | Cartesian coordinate (m) |

*Greek symbols*

| | |
|---|---|
| $\alpha$ | phase volume fraction |
| $\beta$ | volumetric expansion coefficient (1/K) |
| $\gamma$ | liquid fraction |
| $\Delta$ | difference |
| $\mu$ | dynamic viscosity (kg/m s) |
| $\rho$ | density (kg/m$^3$) |

*Subscripts*

| | |
|---|---|
| $i$ | component |
| m | melting |
| ref | reference value |
| w | wall |

is not always intentional, and may be caused, for instance, by thermocouple wires inserted into the enclosure. For this reason, it has become common to monitor the melting process directly, using transparent bases for horizontal cylinders [10], and transparent spherical shells [11], rather than to measure temperatures. Accordingly, the observed location of the solid–liquid interface or the fraction of melted phase in the total amount of the PCM are used as the parameters which characterize the process qualitatively.

Modeling of melting in spherical geometry presents, therefore, a considerable challenge. In addition to the non-linear behavior of the melting front, common to all phase-change problems, we encounter here such phenomena as convection in the melt, volumetric expansion, motion of the solid in the melt, and motion of the liquid in the gap between the solid and the wall of the shell. Due to the difficulties in modeling, it has become common to neglect some of these phenomena and approximate the remaining ones when a numerical solution is attempted.

Works that look into details of the melting process in spherical and horizontal cylindrical enclosures started to appear in the literature in early eighties. A numerical analysis of melting in a horizontal cylinder, performed by Nicholas and Bayazitoglu [12], was the first to consider the effects of solid/liquid density change, while neglecting convective motion in the melt. Moore and Bayazitoglu [11] studied experimentally and numerically melting in a spherical enclosure. Their numerical model included both the descend, or sinking, of the solid phase in the liquid due to the density difference, and fluid motion that contributes to the convective term in the energy equation for the liquid phase. In the numerical solution of Moore and Bayazitoglu [11] the origin of the coordinate system was positioned in the solid region, restricting the modeling of the process from its full completion. Based on the small velocity of descend, the velocity field was modeled by a quasi-steady approach. The gap between the solid and the wall in the lower part of the enclosure was approximated as the Poiseuille flow between two stationary parallel plates. In the experiments, Moore and Bayazitoglu [11] used *n*-octadecane wax in glass spheres. An agreement between the numerical predictions and the experimental results was obtained for the Stefan numbers, *Ste*, of 0.05 and 0.10.

Melting in the spherical geometry has been studied further by Roy and Sengupta [13], who treated analytically the entire melting process. Their method is similar to that proposed by Bareiss and Beer [6] for a horizontal cylinder, but with a different approach to the liquid film between the solid and the wall. The process was assumed to be quasi-steady, no melting was assumed at the upper surface of the solid, and the heat transfer occurred through the liquid film only. Bahrami and Wang [14] also applied the method of [6] to melting in a sphere, neglecting melting at the upper solid surface. Prasad and Sengupta [15] used the results of [6] for the contact zone in their numerical study of melting in a horizontal cylinder.

Roy and Sengupta [16] present a theoretical model of gravity assisted melting in a spherical enclosure, which takes into account natural convection in the melt. The liquid film and the upper liquid zone are solved separately, analytically and numerically, respectively. Melting at the upper surface of the solid is included; however, it is assumed that this surface remains spherical. The cases considered had "the range of parameters encountered in typical solar thermal applications", and in particular $Ste \ll 1$. It is shown that the flow in the upper zone is considerably affected by the motion of the solid core. On the other hand, the melting process is strongly affected by the Grashof number: an increase in *Gr* reduces the effect of the downward motion of the solid core on the flow and melting in

the upper part of the enclosure. Discussing a generalized model for gravity-assisted axisymmetric melting, Roy and Sengupta [17] observe that a "melt distance parameter", which incorporates the Stefan, Archimedes, and Prandtl numbers, determines the order of the liquid film thickness and thus governs the heat transfer expressed by the Nusselt number. Saitoh and Kato [10], who considered a horizontal cylindrical enclosure, concluded that for the small Stefan numbers, the contribution of natural convection to the melting rate is about 10–15%. This contribution becomes significant when the Stefan number increases.

Fomin and Saitoh [18] presented a mathematical model of melting in a spherical enclosure with a non-isothermal wall, showing considerable difference with the previously obtained results for a constant-temperature wall. Their analysis is based on the method developed by Bareiss and Beer [6], with the assumed shape of the solid phase, negligible melting at the upper surface of the solid, close contact melting, quasi-steady process, and lubrication theory approach to the liquid film.

In addition to the simplifications and assumptions listed above, all the works cited herein do not take into account the volume expansion due to melting: they account for the *density* change in order to model solid sinking, but do not address the *volume* change. This, of course, could be done in the simulations only. As for the experiments, the volume increase was accommodated by "risers" [11] or "overflow pipes" [10] connected to the enclosures. Recently, Wilchinsky et al. [19] considered theoretically the volume change in an elastic, i.e. expandable, enclosure. In a rigid shell, however, certain part of the nominal volume should be filled by, say, air. The latter would be either compressed or allowed to leave the shell during the PCM expansion. Accordingly, the initial amount of the solid PCM should be set based on the necessity to accommodate the liquid volume. Thus, questions arise about the initial shape of the solid PCM and its effect on the process. This problem is significant considering the large solid/liquid density changes characteristic for many prospective PCMs, including paraffins.

The present work is an attempt to solve complete transient conservation equations simultaneously for solid PCM, liquid PCM, and air, while allowing for PCM expansion, convection in the fluid media (melted PCM and air), and solid phase motion in the liquid. No a priori assumptions are used for the melting process features and parameters, including shape and behavior of the solid and liquid phases in the lower and upper parts of the enclosure. This approach has been implemented successfully in a recent study by the authors [20], where a PCM-based finned heat sink is considered. Detailed phase fields have been obtained as functions of time, showing evolution of the heat transfer in the system as the phase-change material melts. In search for generalization, dimensional analysis of the results was performed and presented as the Nusselt numbers and melt fractions vs. the Fourier and Stefan numbers and fin parameters. In some cases, the effect of Rayleigh number, *Ra*, also was significant.

In the present work, the same approach is used for a detailed parametric investigation of melting in spherical shells of 40, 60, and 80 mm in diameter, when the wall-temperature is uniform and varies, in different cases, from 2 °C to 20 °C above the mean melting temperature of the PCM. In addition, experiments are performed and their results serve for the validation of the numerical approach. The experimental study is based on the previous investigations by the authors [21,22].

In the following section, a physical model of the problem is introduced, and the numerical procedure is presented in detail and discussed. The experimental results and procedure are described. Then, a comparison is presented of the numerical and experimental results for a test case. We note here that it is common in the literature to compare numerical predictions with the experimental results of Moore and Bayazitoglu [11]. However, as observed by Bahrami and Wang [14] and supported by Roy and Sengupta [16], the numerical solutions do not take into account a considerable thermal resistance of the glass used in the experiments. For this reason, the test numerical case used for validation in the present study includes a shell with the temperature boundary condition applied to its *outer* surface. Then, a detailed parametric investigation is performed. Its findings are followed by a dimensional analysis that leads to generalized results which encompass the cases considered in the present study.

## 2. Numerical study

A physical model of the system is presented in detail below. Then, the computational procedure is discussed.

### 2.1. Physical model

In the present investigation, we explore details of melting in a spherical enclosure of 40, 60, and 80 mm in diameter, at the wall-temperatures of 2, 6, 10, and 20 °C above the mean melting temperature of the PCM. The properties of the PCM are based on a commercially available material, RT27 (Rubitherm GmbH). A real paraffin blend, like RT27, does not have sharply defined "solidus" and "liquidus" temperatures, and its enthalpy is a continuous function of the temperature. In the present work, a melting interval of 28–30 °C is used, as a first step from a "sharp" phase-change analysis to a more realistic representation. The other parameters are: latent-heat 179 kJ/kg, sensible heat capacity in solid/liquid state 2.4/1.8 kJ/kg K, thermal conductivity in solid/liquid state 0.24/0.15 W/m K, constant density of 870 kg/m$^3$ in the solid state, and dynamic viscosity of $3.42 \times 10^{-3}$ kg/m s in the liquid state. Variable density was defined in the liquid state as $\rho = \rho_l/[\beta(T - T_l) + 1]$ for $30\ ^\circ\mathrm{C} < T < 100\ ^\circ\mathrm{C}$, where $\rho_l = 760$ kg/m$^3$, $T_l = 30$ °C, and $\beta = 0.5 \times 10^{-3}$ K$^{-1}$, with linearly varying density in the "mushy" state, from 870 kg/m$^3$ at 28 °C to 760 kg/m$^3$ at 30 °C. It is assumed that both solid and liquid phases are homogeneous and isotropic, and the melting process is axisymmetric. The mol-

ten PCM and the air are incompressible Newtonian fluids, and laminar flow was assumed in both. A density-temperature relation is used for air: $\rho = 1.2 \times 10^{-5}T^2 - 0.01134T + 3.4978$.

In the initial state, the solid PCM fills 85% of the enclosed space. This is done in order to accommodate a significant increase in the PCM volume during the solid–liquid phase transition, due to a large difference in solid and liquid density that exists in reality. From above, the PCM is exposed to air. In the simulations, the initial temperature of the whole system is 23 °C, i.e. the PCM is slightly subcooled.

### 2.2. Computational procedure

The numerical approach makes it possible to calculate the processes that occur inside the solid PCM (conduction), liquid PCM (convection), and air (convection) simultaneously, and to account for the phase-change, moving boundary due to the variation of the PCM volume, and solid phase motion in the melt. Based on the axial symmetry of the physical model, a computational domain was defined, as shown in Fig. 1.

In order to describe the PCM–air system with a moving internal interface but without inter-penetration of the two media,[1] the so-called "volume-of-fluid" (VOF) model has been used. In this model, if the $n$th fluid's volume fraction in the computational cell is denoted as $\alpha_n$, then the following three conditions are possible: if $\alpha_n = 0$ the cell is empty of the $n$th fluid; if $\alpha_n = 1$ the cell is full of the $n$th fluid; and if $0 < \alpha_n < 1$ the cell contains the interface between the $n$th fluid and one or more other fluids. Thus, the variables and properties in any given cell are either purely representative of one of the media, or representative of a mixture of the media, depending upon the volume fraction values.

For the phase-change region inside the PCM, enthalpy-porosity approach [23–25] is used, by which the porosity in each cell is set equal to the liquid fraction in that cell. Accordingly, the porosity is zero inside fully solid regions. This approach has been successfully implemented by the authors for a PCM-based finned heat sink [20].

Therefore, the governing conservation equations used here for the PCM–air system are:

– continuity

$$\frac{\partial \alpha_n}{\partial t} + u_i \frac{\partial \alpha_n}{\partial x_i} = 0 \tag{1}$$

– momentum

$$\frac{\partial}{\partial t}(\rho u_i) + \frac{\partial}{\partial x_j}(\rho u_j u_i) = \mu \frac{\partial^2 u_i}{\partial x_j \partial x_j} - \frac{\partial p}{\partial x_i} + \rho g_i + S_i \tag{2}$$

[1] The term "medium" is used here instead of "phase" in order to prevent confusion with the solid and liquid phases of the PCM.

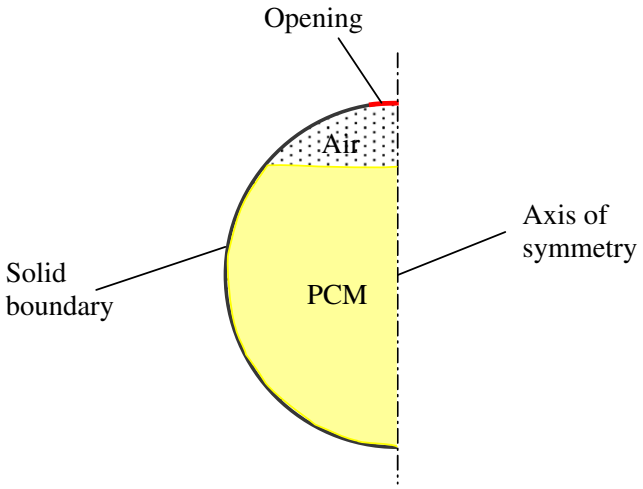


Fig. 1. The computational domain.

– energy

$$\frac{\partial}{\partial t}(\rho \hbar) + \frac{\partial}{\partial x_i}(\rho u_i \hbar) = \frac{\partial}{\partial x_i}\left(k \frac{\partial T}{\partial x_i}\right) \tag{3}$$

where $\alpha_n$ is the $n$th fluid's volume fraction in the computational cell, $\rho$ is the density, $k$ is the thermal conductivity, $\mu$ is the dynamic viscosity, $S_i$ is the momentum source term, $u_i$ is the velocity component, $x_i$ is a Cartesian coordinate, and $\hbar$ is the specific enthalpy. The latter is defined as a sum of the sensible enthalpy, $\hbar_s = \hbar_{ref} + \int_{T_{ref}}^{T} c_p \, dT$, and the enthalpy change due to the phase-change $\gamma L$, where $\hbar_{ref}$ is the reference enthalpy at the reference temperature $T_{ref}$, $c_p$ is the specific heat, $L$ is the specific enthalpy of melting (latent-heat of the material), and $\gamma$ is the liquid fraction during the phase-change which occurs over a range of temperatures $T_s < T < T_l$, defined by the following relations:

$$\gamma = 0 \quad \text{if } T < T_s, \quad \gamma = 1 \quad \text{if } T > T_l,$$
$$\gamma = \frac{T - T_s}{T_l - T_s} \quad \text{if } T_s < T < T_l \tag{4}$$

The source term $S_i$ in the momentum equation, Eq. (2), is given by:

$$S_i = -A(\gamma) u_i \tag{5}$$

where $A(\gamma)$ is the "porosity function" defined by Brent et al. [24]. Definition of $A(\gamma)$ makes the momentum equation "mimic" Carman–Kozeny equations for flow in porous media:

$$A(\gamma) = \frac{C(1-\gamma)^2}{\gamma^3 + \varepsilon} \tag{6}$$

where $\varepsilon = 0.001$ is a small computational constant used to avoid division by zero, and $C$ is a constant reflecting the morphology of the melting front. This constant is a large number, usually $10^4$–$10^7$. A value of $C = 10^5$ has been used in the previous study [20], where its effect was discussed. The same value of $C$ is adopted herein.

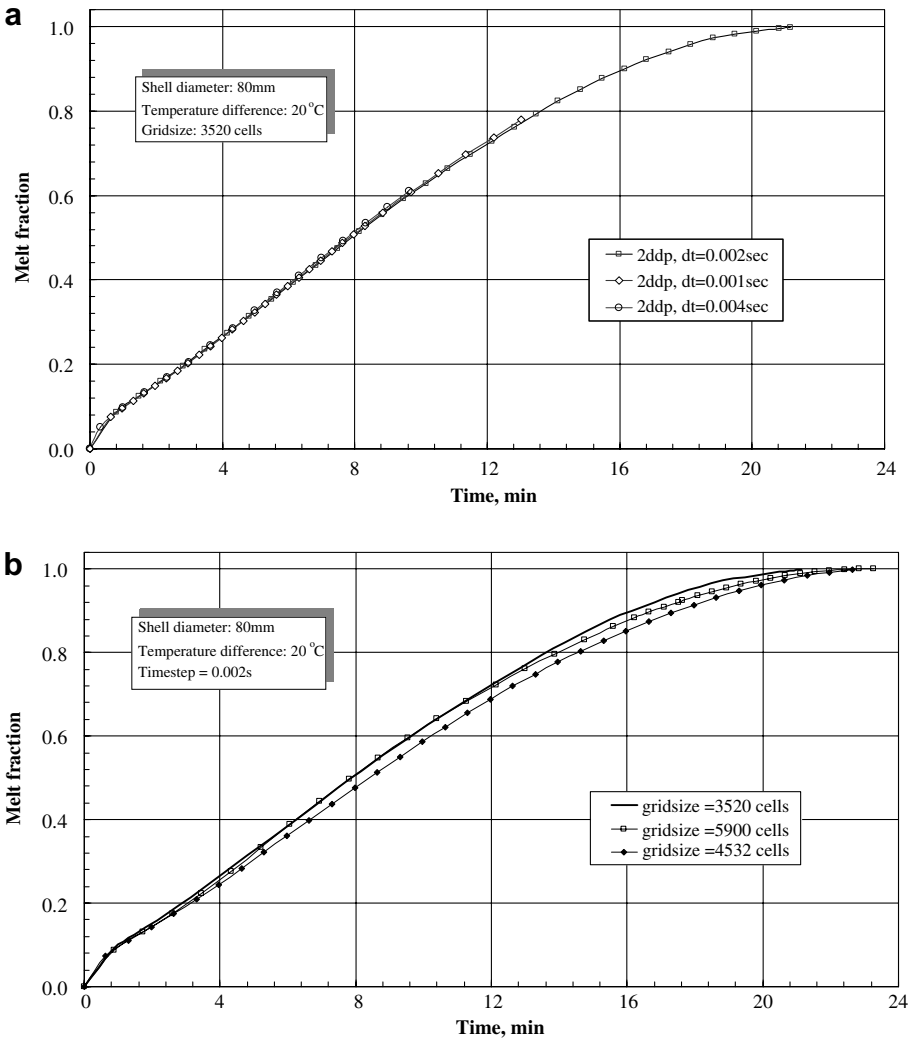


Fig. 2. Time-step and grid dependence of the numerical solution.

The numerical solution has been obtained using the Fluent 6.0 software. The effects of time step and grid size on the solution were carefully examined in preliminary calculations, as presented in Fig. 2. In particular, the time-step was as small as 0.001, 0.002 (chosen), and 0.004 s. As appears from the results of Fig. 2a, the results obtained for melt fraction became practically independent of the time step, through the whole process, i.e. from $t = 0$ to the complete melting of the PCM. The grid was built using the Gambit software, with special attention paid to the PCM–air interface in the initial state. The grid size was chosen after careful examination of the results of a grid refinement process. Fig. 2b shows the results for three different grid sizes, namely 3520 (chosen), 4532, and 5900 cells. One can see that the differences, once again presented for the whole process, are rather small. Convergence of the solution was checked at each time step, with the convergence criterion of $10^{-5}$ for the velocity components and continuity, and criterion of $10^{-8}$ for energy.

The authors used a Dell PowerEdge 2600 computer, which features two 3.20 GHz Intel Xeon processors and is scalable to 12 Gb of PC2100 DDR SDRAM. The CPU time was rather considerable, of about 300–400 s per second of physical time. Thus, a typical run took a few days.

## 3. Experimental set-up and procedure

In the present study, the experiments are designed specifically to meet the conditions explored in the numerical investigation. The inner diameter of the spherical shell is 80 mm. The amount of the PCM is the same as in the simulations. The solid phase occupies initially 85% of the volume, having a flat top. In order to achieve a desired shape, the shell is filled gradually with a liquid PCM allowing the latter to solidify at each stage. This process is performed at the reduced ambient pressure, in order to prevent air entrapment in the PCM. The material used in the experimental study was the RT27 paraffin wax (Rubitherm GmbH), claimed to be suitable for heat-storage applications.

The experimental set-up, shown schematically in Fig. 3, has been extensively described in [21,22]. Experiments are

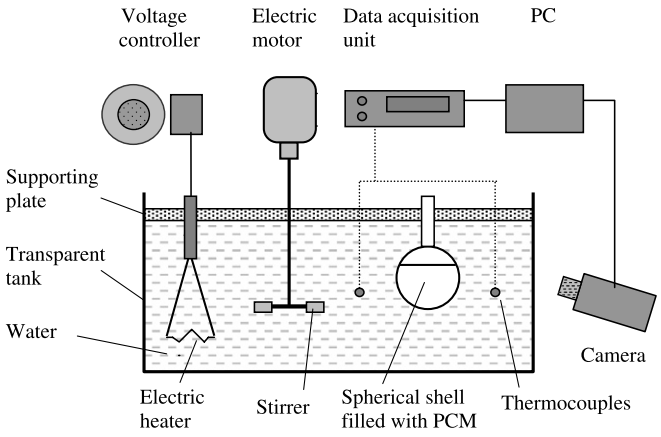


Fig. 3. Experimental set-up.

performed in a transparent tank, filled with water. In order to keep water temperature at a certain level, an electric heater is used, and its power is adjusted using a variable voltage controller. In order to ensure uniform temperature of water inside the tank, a mechanical turbine-type stirrer is used. In a typical experiment, a spherical shell filled with the solid PCM is placed into the water. The experiment continues until the PCM has melted completely. The shell has a "neck", like in [11], that lets the air out when the PCM expands during its melting.

Thermocouples are used to monitor the temperature of water at different locations inside the tank. All thermocouples are connected to a PC through a data acquisition unit. Typical results of the temperature measurements, including that of the PCM, were presented and discussed in [21] and are not included herein. We should note, however, that temperature measurements inside the PCM could alter the results, because the solid phase becomes suspended on the thermocouple wires and does not sink, as modeled by Khodadadi and Zhang [8]. For this reason, visualization of melting in a glass shell has been chosen as the major method of investigation. Melting images are recorded by a digital camera at various stages of the process. Then, these images are analyzed and the experimental values of the melt fraction are calculated at various time instants. The results are used for validation of the numerical approach, as reported in the next section.

## 4. Results and discussion

This section presents first a comparison of the experimental results with the results of a simulation performed for validation purposes. Then, a detailed parametric study of melting is reported and discussed, and results of the dimensional analysis are presented.

### 4.1. Validation of the numerical model

Fig. 4 shows the measured and simulated melt fractions vs. time for a spherical enclosure 80 mm in diameter, with the wall thickness of 2 mm, in the environment at 10 °C higher than the mean melting temperature of the PCM. As discussed in Section 1, it is essential for validation to model numerically a shell with a given wall thickness, thus taking into account a considerable thermal resistance of the glass.

One can see that the melting time is slightly shorter in the simulation. We note that in the experiment the temperature of the water was kept fixed, while in the simulation the same value was set on the outer surface of the shell.

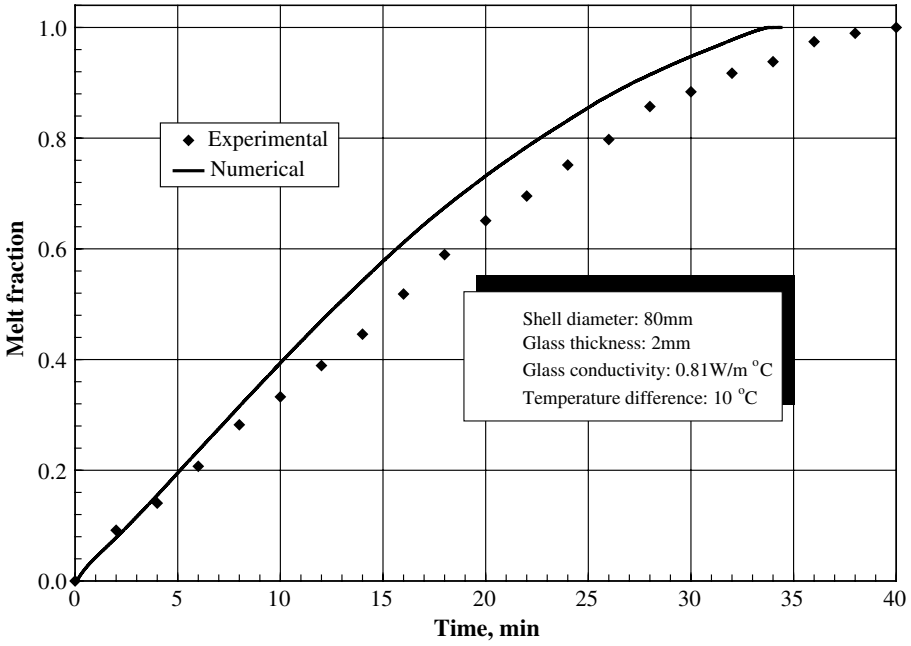


Fig. 4. Comparison of the experimental and numerical melt fractions.

Thus, an additional thermal resistance, albeit small, existed in the experiments. Also, the modeled glass conductivity, taken from the literature, could be higher than the actual one, which had not been measured directly. All in all, one can conclude that the agreement between the experimental and simulated values is very good.

Furthermore, it appears from Fig. 5 that good agreement is achieved not only in overall parameters, but also in the details of the melting process. Fig. 5a shows typical results of visualization for paraffin melting, as obtained during the experiments, at 2, 5, 10, 15, 20 and 25 min since the start of the process. One can see from the figure that the solid phase typically descends. This result is in very good agreement with the literature. The label on the shell can be used to observe the process of PCM melting.

Fig. 5b shows examples of the simulated phase distribution for the same time instants as in Fig. 5a. Fig. 5c illustrates the volumetric expansion of the PCM associated with melting, showing the resulting rise of the PCM level in the shell between 2 and 25 min that passed since the start. One can see a good agreement with the experimental findings. It has been concluded, therefore, that the numerical approach yields valid results both qualitatively and quantitatively.

### 4.2. Detailed parametric study

Figs. 6 and 7 show the results for the melt fractions and mean heat fluxes, respectively. Three shell diameters are explored: 40, 60, and 80 mm. The temperature differences are 2 °C, 6 °C and 10 °C above the mean melting temperature of the PCM. For the 80 mm shell, an additional result for $\Delta T = 20$ °C is also shown.

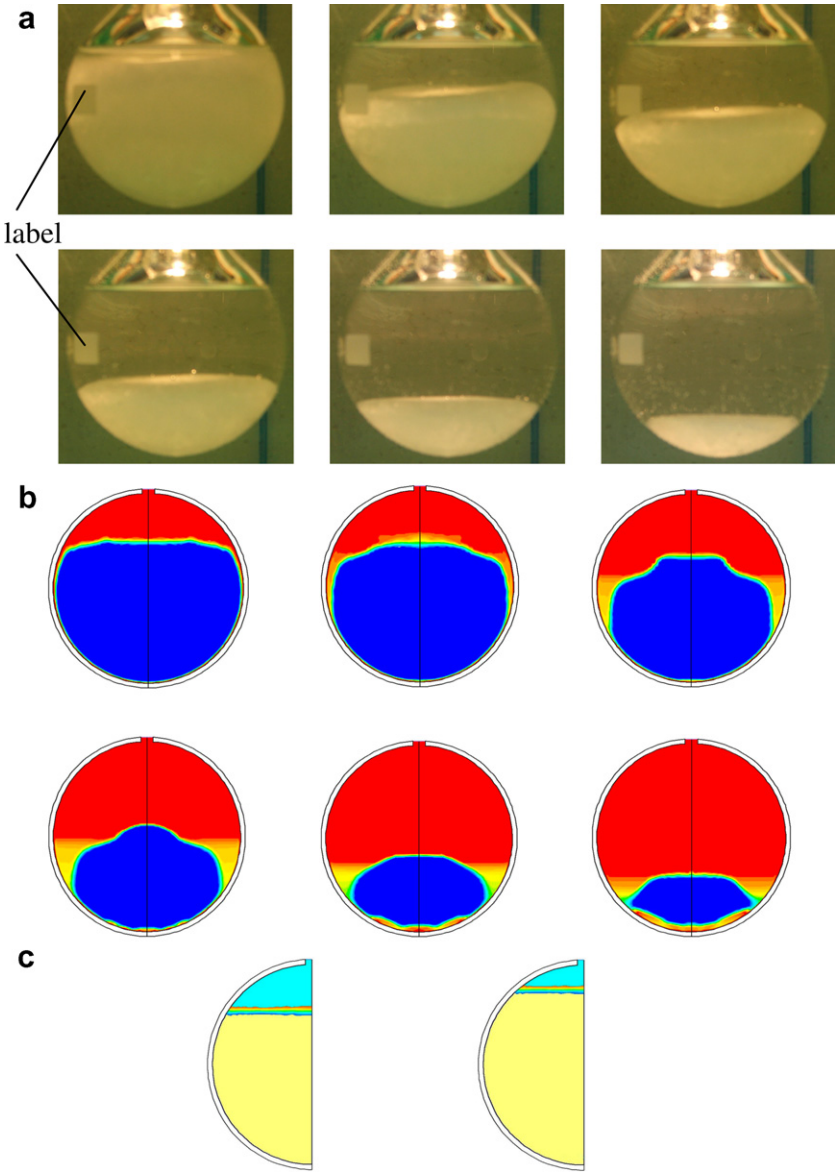


Fig. 5. Experimental and numerical melting patterns: (a) experimental; (b) numerical – solid phase; (c) numerical – interface rise.

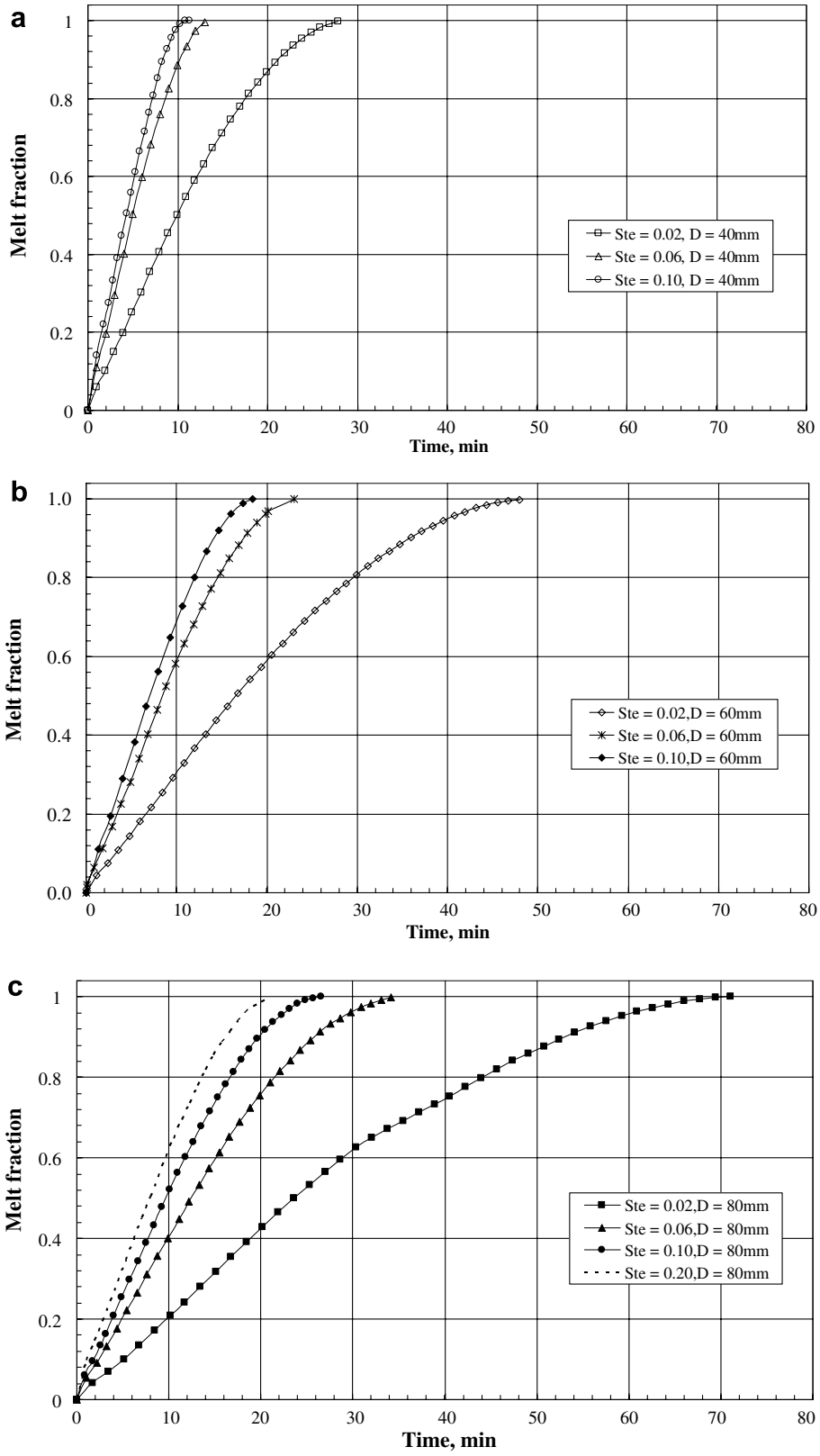


Fig. 6. Melt fractions for different shell diameters: (a) shell diameter 40 mm; (b) shell diameter 60 mm; (c) shell diameter 80 mm.

As expected, for each shell diameter the melt fraction increases more rapidly when the temperature difference is higher. When the melt fraction reaches unity, Fig. 6a–c, the mean heat flux drops almost to zero, as illustrated in Fig. 7a–c, corresponding to heat transfer to the liquid PCM only. Figs. 6 and 7 also show that for the same

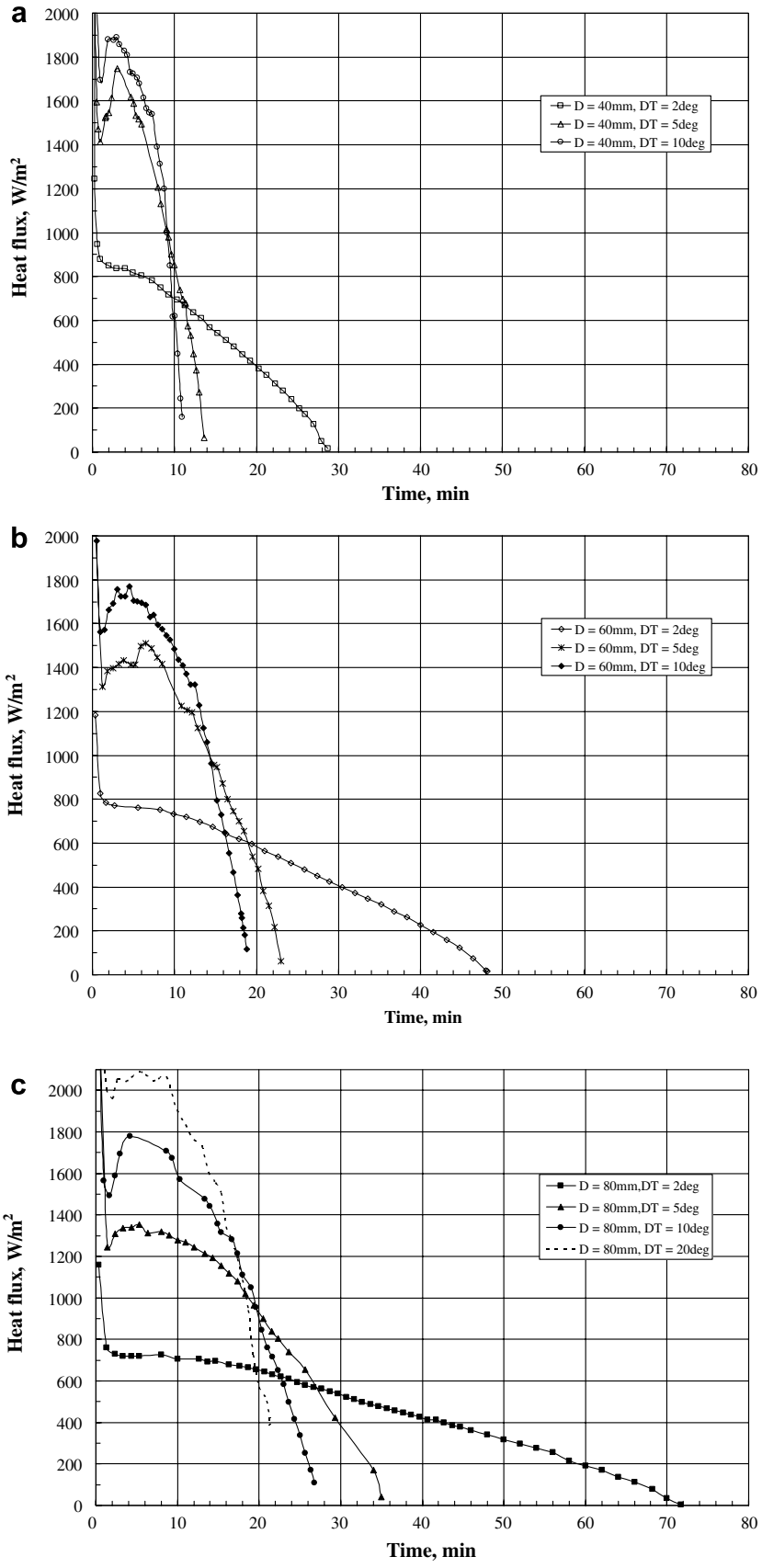


Fig. 7. Mean heat fluxes from the wall for different shell diameters: (a) shell diameter 40 mm; (b) shell diameter 60 mm; (c) shell diameter 80 mm.

temperature difference, full melting is reached more rapidly in a shell of a smaller diameter. It is important to note that for the shell 80 mm in diameter and the temperature difference of $\Delta T = 10$ °C, the melting time was about 27 min, see Figs. 6c and 7c. However, in the test case, Fig. 4, where glass thickness was accounted for, the melting time was as long as about 34 min in the otherwise same conditions. This difference is consistent with the analysis of Bahrami and Wang [14], discussed in Section 1.

One can see from Fig. 6 that the melt fraction grows monotonically with time in all cases considered. On the other hand, Fig. 7 shows a rather different behavior of the mean heat flux. At first, it is very high due to the low thermal resistance associated with the initially thin molten layer. As the latter grows, the heat flux decreases sharply. Then, this decrease is stopped, and in certain cases it is even reversed. A difference is observed between the case with a very low temperature difference, $\Delta T = 2$ °C, and the other cases. In the former, the heat flux decreases monotonically throughout the melting process. In the latter, an increase in the heat flux is observed. This increase may be attributed to motion initiated in the liquid phase, and is similar to that observed by Pal and Joshi [26] in a side-heated rectangular enclosure. However, in their study the motion was due to temperature-driven natural convection, while here it is caused also by the sinking solid phase.

While Figs. 6 and 7 present results for different shell diameters separately, Fig. 8 brings together the results for the different diameters at the same temperature difference, $\Delta T = 6$ °C ($Ste = 0.06$). Similar trends are observed in the melt fraction and heat flux evolution. In addition, one can see that the increase in the heat flux is sharper for a smaller shell diameter, but its duration is shorter.

Fig. 9 shows an example of simulation results for the melt fraction evolution throughout the whole simulation process. The results are presented for the 80 mm shell at $\Delta T = 2$ °C ($Ste = 0.02$). One can see that the solid fraction sinks in the molten PCM. This result, as well as the observed shape of the solid, is in excellent agreement with the experimental results from the literature.

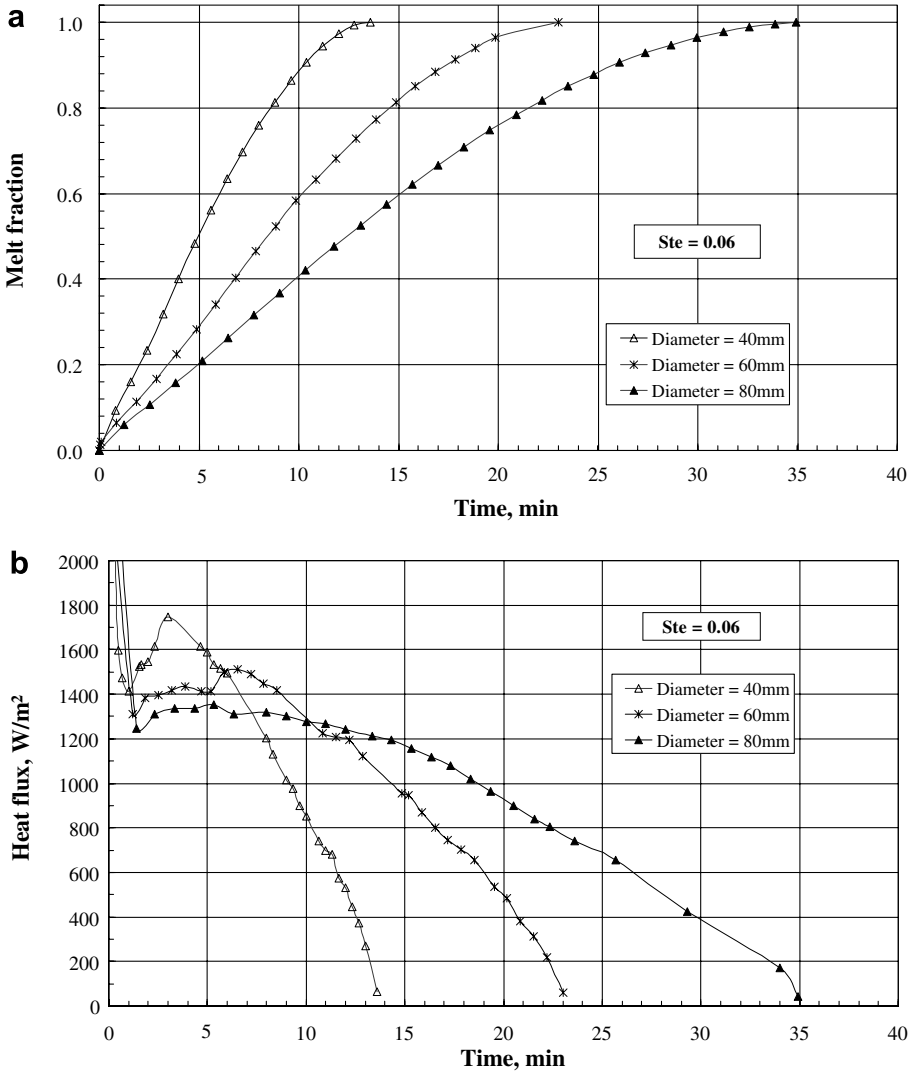


Fig. 8. Comparison of the results for the same temperature difference: (a) melt fractions and (b) mean heat fluxes.

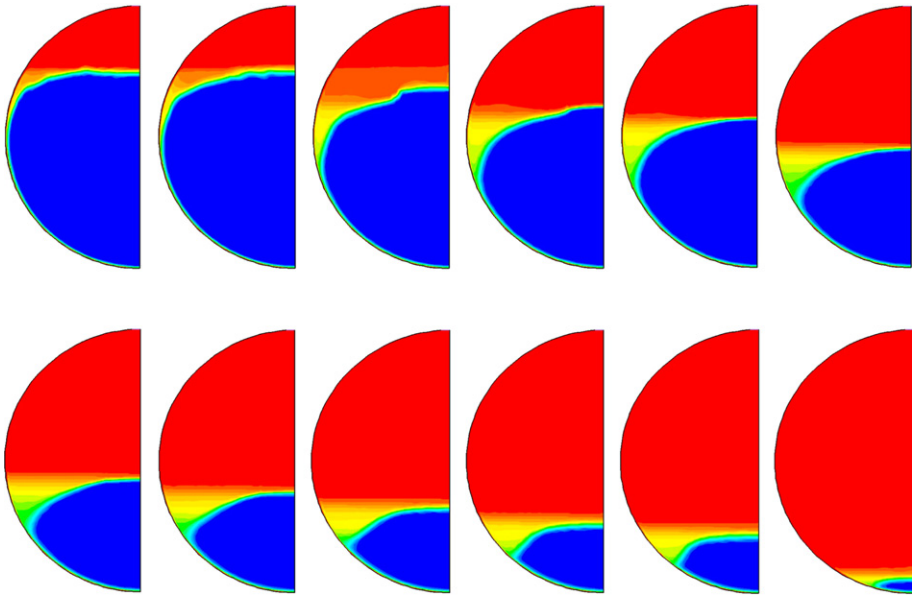

Fig. 9. Detailed phase fields throughout the melting process, for $\Delta T = 2$ °C.

Fig. 10 presents a typical example of the simulated flow fields at various locations inside the enclosure. The flow patterns are shown for the case with $D = 80$ mm and $\Delta T = 6$ °C, at $t = 400$ s after the melting process has been initiated. Fig. 10a shows motion of air in the bubble above the PCM. As mentioned above, the air is allowed to leave the enclosure through the opening shown in Fig. 1. Hence, air flows out of the enclosure as a result of PCM expansion, and both its volume and mass decrease slowly during the process. The motion of air is characterized also by vortices caused by shell-PCM temperature differences and by the motion in the adjoining liquid PCM.

Fig. 10b shows that in the upper part of the melt, natural convection is initiated by the temperature difference between the heated wall and the relatively cold solid phase. As a result, the liquid rises along the wall and moves towards the axis of symmetry of the enclosure, returning back just above the solid, forming a clockwise vortex in the cross-section shown in Fig. 10b.

In the lower part of the enclosure, Fig. 10c shows a thin liquid layer between the sinking solid and the shell. Thus, the simulation succeeds to model directly the "close-contact-melting" phenomenon assumed for the cylindrical and spherical geometries by Bareiss and Beer [6] and Fomin and Saitoh [18], respectively. This phenomenon is characterized by a liquid layer which takes the molten PCM into the upper part of the enclosure while the solid melts continuously and moves towards the boundary, "squeezing" the liquid. We note, however, that the simulated layer is more realistic than that assumed in the past, when it was modeled as a flow in the gap between two stationary plates. In the simulation, the no-slip condition is satisfied on both the shell and the solid. As the latter moves downwards, the velocity near its surface is in the opposite direction to that of the flow that takes the molten PCM to the region above the solid. One can see from Fig. 10b and c that the layer leaves the gap and joins smoothly the vortex described above. It may be concluded that the layer itself contributes to creation of this vortex, in addition to natural convection. We note here that the layer between the solid and the wall, and its interaction with the vortex in the melt above the solid, have been observed to follow in general the same patterns in all cases simulated in the present study. However, there are indications that the layer details are different for higher temperature differences between the wall and the solid. This point needs further investigation.

### 4.3. Dimensional analysis

The results presented in Figs. 6–8 and discussed above show that similar behavior characterizes the melting process under different geometrical and thermal parameters of the system. It is thus worth to attempt a dimensional analysis in order to obtain generalized results.

Two dependent dimensionless parameters are used: the melt fraction of the PCM, defined as the current melted mass divided by the total mass of the PCM, and the Nusselt number, which is defined as

$$Nu = \frac{q''}{\Delta T} \cdot \frac{R}{k} \tag{7}$$

i.e. it is based on the mean heat flux, $q''$, the temperature difference between the wall and the PCM mean melting temperature, $\Delta T$, shell radius $R$, and thermal conductivity of the PCM, $k$. We note here that the melt fraction reflects rather accurately the amount of heat stored in the system up to a certain moment, while the Nusselt number shows an instantaneous picture of the process at the same

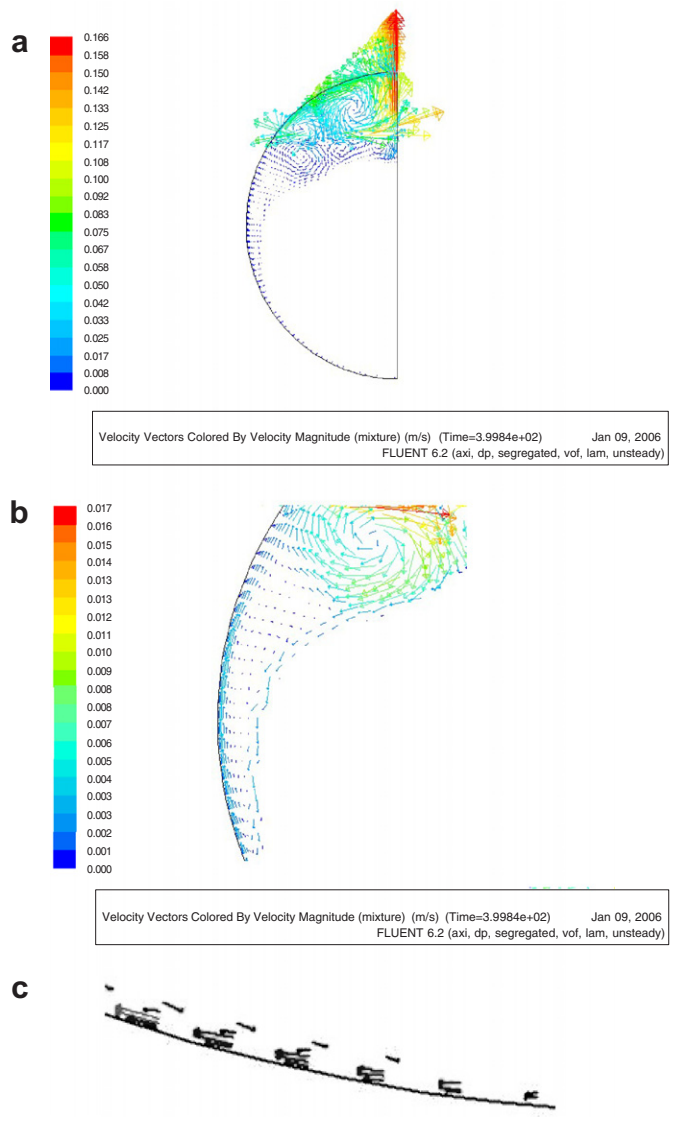


Fig. 10. Examples of the flow field at $t = 400$ s, for $D = 80$ mm and $\Delta T = 6$ °C: (a) in the air above the PCM; (b) vortex flow inside the melt and liquid layer coming from below; (c) thin liquid layer in the lower part of the shell.

moment. Hence, these two parameters supplement one another.

The dimensionless parameters that define the process can be obtained from the momentum and energy equations, Eqs. (2) and (3), if the latter are presented in a form given by Lacroix [27]. The dimensionless conservation equations contain the following dimensionless groups:

– the Fourier number

$$Fo = (k/\rho c_p)(t/R^2) \tag{8}$$

where $c_p$ is the specific sensible heat of the PCM, and the shell radius, $R = D/2$, is chosen as the characteristic length;

– the Stefan number

$$Ste = c_p \Delta T / L \tag{9}$$

where $\Delta T$ is the difference between the wall-temperature, $T_w$, and the PCM mean melting temperature, $T_m$, and $L$ is the specific heat of melting. In the present study Stefan number varies from about 0.02 ($\Delta T = 2$ °C) to 0.10 ($\Delta T = 10$ °C), and in an additional case it reaches 0.20 ($\Delta T = 20$ °C for $D = 80$ mm);

– the Grashof number

$$Gr = \frac{g\rho^2 \beta \Delta T R^3}{\mu^2} \tag{10}$$

where $\beta$ is the volumetric expansion coefficient introduced earlier. The Grashof numbers vary from about $3 \times 10^4$ to $2.5 \times 10^6$ under the conditions of the present study.

– the Prandtl number

$$Pr = c_p \mu / k \tag{11}$$

The Prandtl number is about 35 for the material used in the present study, i.e. $Pr \gg 1$.

A combination of the Fourier and Stefan numbers would have been sufficient for melting accompanied by conduction only. The examples presented in Fig. 11 were chosen purportedly, to show the behavior of the melt fraction for the same shell diameter, i.e. the same Fourier number in different cases (Fig. 11a), and for the same temperature difference between the wall and the PCM, i.e. a constant Stefan number (Fig. 11b). One can see from Fig. 11 that when the melt fraction is presented vs. the product, $FoSte$, of the Fourier and Stefan numbers, no generalization is achieved, although the different curves come closer together, especially in Fig. 11b as compared to Fig. 8a.

Careful application of the dimensionless groups introduced above leads to the generalized results presented in Figs. 12 and 13. Fig. 12 shows the melt fraction vs. a combination of the Fourier, Stefan, and Grashof numbers, namely $FoSte^{1/3}Gr^{1/4}$, for *all* cases considered in the present study (compare $FoSte^{3/4}Gr^{1/4}$ obtained for a cylindrical enclosure by Saitoh and Kato [10]). One can see that all curves, except that for $Ste = 0.2$, practically merge into a single curve. In our opinion, the higher dimensionless melting time of about 10–20% for $Ste = 0.2$ results from the above-mentioned changes in the melting process that characterize higher given temperature differences between the wall and the PCM, and in particular larger thickness of the lower liquid layer and its distortion. Thus, we conclude that the generalization is full for $Ste \leqslant 0.1$, which corresponds here to $\Delta T \leqslant 10$ °C.

Analysis of the results of Fig. 12 yields the following expression for the melt fraction:

$$\mathrm{MF} = 1 - \left(1 - \frac{FoSte^{1/3}Gr^{1/4}}{1.9}\right)^{3/2} \tag{12}$$

This correlation, also shown in Fig. 12, is valid for the range of parameters explored in the present study, and in particular for $0.02 \leqslant Ste \leqslant 0.10$ and $Pr \gg 1$.

Fig. 13a shows the dimensionless mean heat flux from the wall vs. the same combination of the Fourier, Stefan,

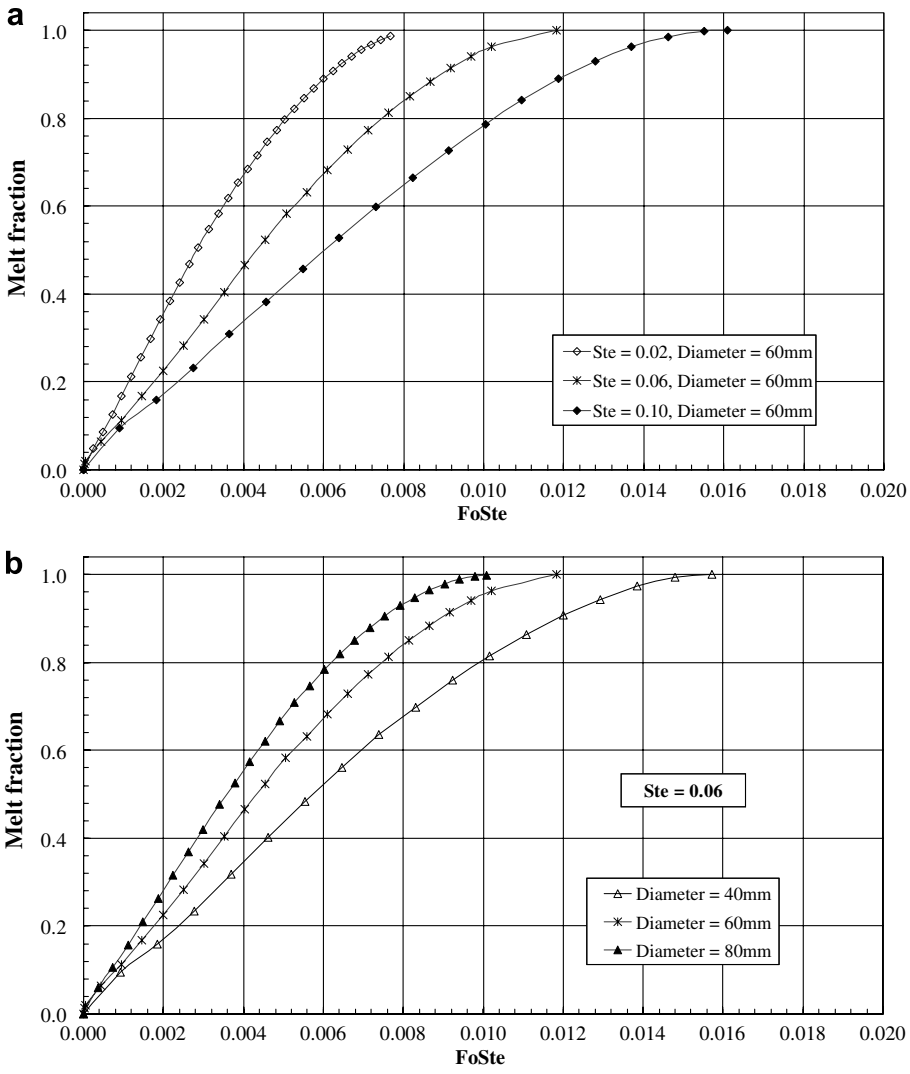


Fig. 11. Examples of the results presented vs. a product of the Fourier and Stefan numbers: (a) melt fractions vs. *FoSte* for the results of Fig. 6b (the same *Fo* for all cases); (b) melt fractions vs. *FoSte* for the results of Fig. 8a (*Ste* = const).

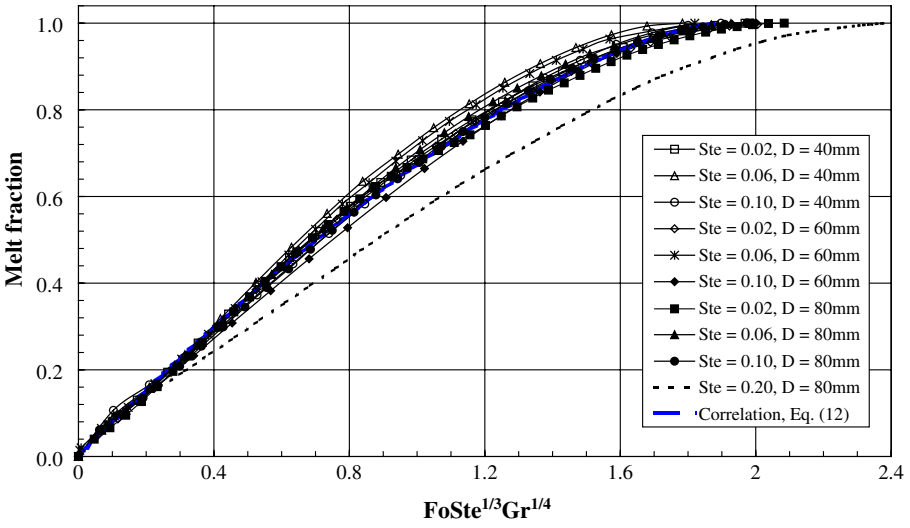


Fig. 12. Generalized results for all simulated cases: melt fractions.

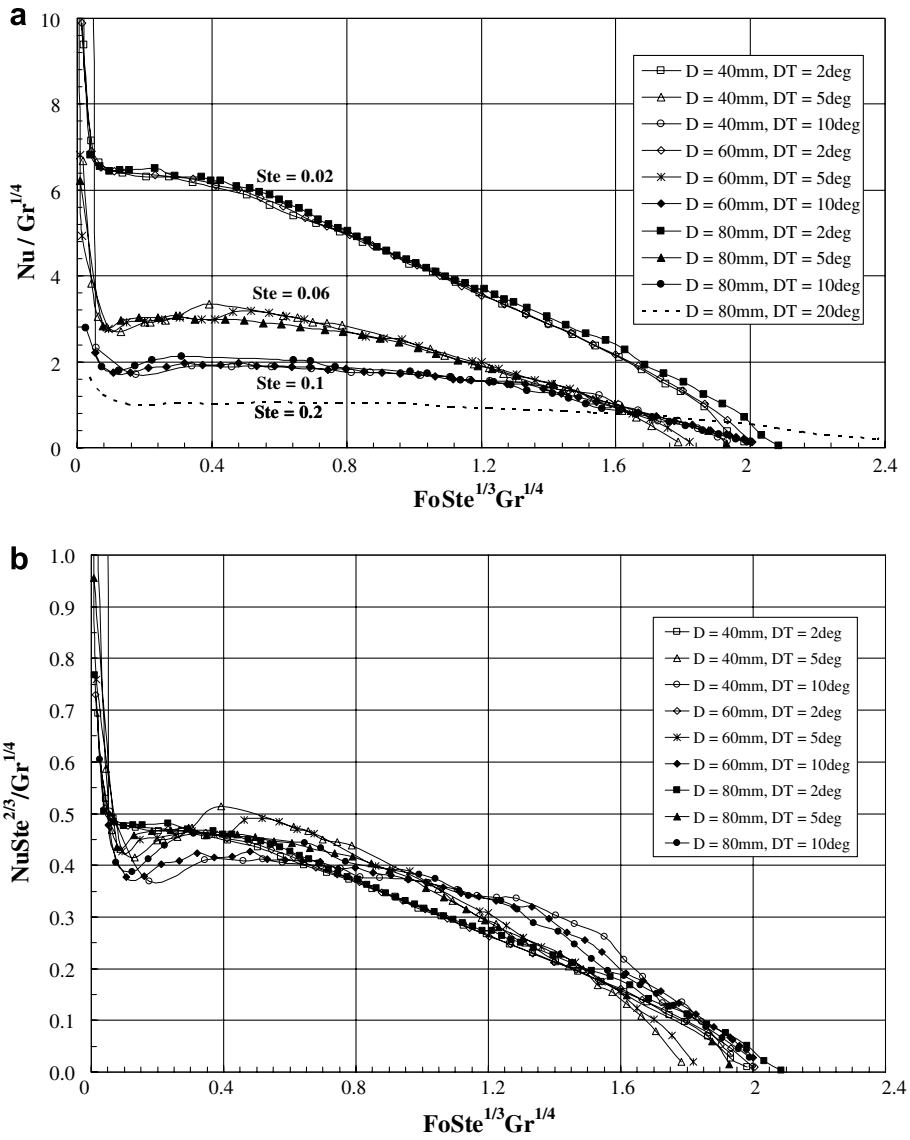


Fig. 13. Generalized results for all simulated cases: Nusselt numbers: (a) with the Stefan number as a parameter and (b) *Nu* normalized with *Ste*.

and Grashof numbers, $FoSte^{1/3}Gr^{1/4}$. The Nusselt number is normalized using the Grashof number. The exponent of *Gr* has been chosen based on the laminar natural convection under the constant-wall-temperature conditions. One can see that distinct curves are formed corresponding to the different values of the Stefan number. Finally, Fig. 13b shows that these curves can be further merged when the Nusselt number is additionally normalized using the Stefan number.

The results of the present study have been obtained for the cases in which air was allowed to flow out of the enclosure to accommodate the PCM expansion. In reality, the shell would rather be sealed, and the air compressed. Also, it has been assumed that the PCM–air interface is initially horizontal and flat. In real conditions, its shape will be determined by the solidification process. The authors are planning to address these points in a future study. However, it is our belief that the trends discovered in the present study are quite general, and the results of the analysis performed herein will be valid also when additional features are taken into account.

## 5. Closure

In the present study, the process of melting of a phase-change material (PCM) in spherical geometry has been explored experimentally and numerically. Transient numerical simulations were performed using the Fluent 6.0 software. Melting temperature of the PCM was incorporated in the simulations along with its other properties, including the latent and sensible specific heat, thermal conductivity and density in solid and liquid states. The experimental study included visualization of the melting process. The material used was a commercially available paraffin wax, which is manufactured to be used mainly in latent-heat-based heat storage systems.

The simulations provided detailed phase and flow fields inside the system which were compared with the experimental results and discussed in the paper. To the best of our knowledge, some inherent features of the process have been modeled directly and simultaneously for the first time, including the PCM volume increase due to the phase-change, solid phase motion in the melt, and the liquid layer in the lower part of the enclosure.

Dimensional analysis of the results was performed and presented as the mean Nusselt numbers and PCM melt fractions vs. an appropriate combination of the Fourier, Stefan, and Grashof numbers. This analysis led to a generalization which encompasses the cases considered herein. This generalization is presented as a correlation applicable within a specified range of parameters which were studied currently.

## References

[1] S. Fukusako, M. Yamada, Melting heat transfer inside ducts and over external bodies, Exp. Therm. Fluid Sci. 19 (1999) 93–117.
[2] H. Koizumi, Time and spatial heat transfer performance around an isothermally heated sphere placed in a uniform, downwardly directed flow (in relation to the enhancement of latent heat storage rate in a spherical capsule), Appl. Therm. Eng. 24 (2004) 2583–2600.
[3] H. Ettouney, H. El-Dessouky, A. Al-Ali, Heat transfer during phase change of paraffin wax stored in spherical shells, J. Sol. Energ. Eng. 127 (2005) 357–365.
[4] K.T. Adref, I.W. Eames, Experiments on charging and discharging of spherical thermal (ice) storage elements, Int. J. Energ. Res. 26 (2002) 949–964.
[5] I.W. Eames, K.T. Adref, Freezing and melting of water in spherical enclosures of the type used in thermal (ice) storage systems, Appl. Therm. Eng. 22 (2002) 733–745.
[6] ] M. Bareiss, H. Beer, An analytical solution of the heat transfer process during melting of an unfixed solid phase change material inside a horizontal tube, Int. J. Heat Mass Transfer 27 (1984) 739–746.
[7] ] H. Rieger, U. Projahn, M. Bareiss, H. Beer, Heat transfer during melting inside a horizontal tube, J. Heat Transfer 105 (1983) 226–234.
[8] J.M. Khodadadi, Y. Zhang, Effects of buoyancy-driven convection on melting within spherical containers, Int. J. Heat Mass Transfer 44 (2001) 1605–1618.
[9] K. Katayama, Akio Saito, Y. Utaka, Akihiro Saito, H. Matsui, H. Maekawa, A.Z.A. Saifullah, Heat transfer characteristics of the latent heat thermal energy storage capsule, Sol. Energ. 27 (1981) 91–97.
[10] T. Saitoh, K. Katoh, Experiment on melting in heat storage capsule with close contact and natural convection, Exp. Therm. Fluid Sci. 6 (1993) 273–281.
[11] F.E. Moore, Y. Bayazitoglu, Melting within a spherical enclosure, J. Heat Transfer 104 (1982) 19–23.
[12] D. Nicholas, Y. Bayazitoglu, Heat transfer and melting front within a horizontal cylinder, J. Sol. Energ. Eng. 102 (1980) 229.
[13] S.K. Roy, S. Sengupta, The melting process within spherical enclosures, J. Heat Transfer 109 (1987) 460–462.
[14] P.A. Bahrami, T.G. Wang, Analysis of gravity and conduction-driven melting in a sphere, J. Heat Transfer 109 (1987) 806–809.
[15] A. Prasad, S. Sengupta, Numerical investigation of melting inside a horizontal cylinder including the effects of natural convection, J. Heat Transfer 109 (1987) 803–806.
[16] S.K. Roy, S. Sengupta, Gravity-assisted melting in a spherical enclosure: effects of natural convection, Int. J. Heat Mass Transfer 33 (1990) 1135–1147.
[17] S.K. Roy, S. Sengupta, A generalized model for gravity-assisted melting in enclosures, J. Heat Transfer 112 (1987) 804–808.
[18] S.A. Fomin, T.S. Saitoh, Melting inside a spherical capsule with non-isothermal wall, Int. J. Heat Mass Transfer 42 (1999) 4197–4205.
[19] A.V. Wilchinsky, S.A. Fomin, T. Saitoh, Contact melting inside an elastic capsule, Int. J. Heat Mass Transfer 45 (2002) 4097–4106.
[20] V. Shatikian, G. Ziskind, R. Letan, Numerical investigation of a PCM-based heat sink with internal fins, Int. J. Heat Mass Transfer 48 (2005) 3689–3706.
[21] L. Katsman, Melting and solidification of a phase-change material (PCM), Graduation Project 16-04, Heat Transfer Laboratory, Department of Mechanical Engineering, Ben-Gurion University of the Negev, June 2004.
[22] E. Assis, L. Katsman, G. Ziskind, R. Letan, Experimental and numerical investigation of phase change in a spherical enclosure, in: Proceedings of the fourth European Thermal Sciences Conference, Birmingham, UK, March 2004.
[23] V.R. Voller, M. Cross, N.C. Markatos, An enthalpy method for convection/diffusion phase change, Int. J. Numer. Meth. Eng. 24 (1987) 271–284.
[24] A.D. Brent, V.R. Voller, K.J. Reid, Enthalpy-porosity technique for modeling convection-diffusion phase change: application to the melting of a pure metal, Numer. Heat Transfer 13 (1988) 297–318.
[25] V.R. Voller, An overview of numerical methods for solving phase-change problems, Advances in Numerical Heat Transfer, vol. 1, Taylor & Francis, 1996 (Chapter 9).
[26] D. Pal, Y.K. Joshi, Application of phase-change materials to thermal control of electronic modules, J. Electron. Packaging 119 (1997) 40–50.
[27] M. Lacroix, Modeling of latent heat storage systems, in: İ. Dinçer, M.A. Rosen (Eds.), Thermal Energy Storage Systems Applications, John Wiley & Sons, Chichester, 2002 (Chapter 7).